

PAPER • OPEN ACCESS

Li⁺ diffusion in crystalline lithium silicides: influence of intrinsic point defects

To cite this article: Christoph Kirsch *et al* 2025 *J. Phys. Energy* **7** 025003

View the [article online](#) for updates and enhancements.

You may also like

- [Suppressing surface segregation by introducing lanthanides to enhance high-temperature oxygen evolution reaction activity and durability](#)
Jingwei Li, Zichao Wu, Yuxiang Shen *et al.*
- [Toward zero-excess lithium sulfur batteries: a systematic cell parameter study](#)
Joshua H Cruddos, James B Robinson, Paul R Shearing *et al.*
- [Investigating charge dynamics at lead halide perovskite single crystal surfaces](#)
Birgit Kammlander, Alberto García-Fernández, Sebastian Svanström *et al.*



PAPER

OPEN ACCESS

RECEIVED
26 August 2024REVISED
17 December 2024ACCEPTED FOR PUBLICATION
6 January 2025PUBLISHED
16 January 2025

Original Content from
this work may be used
under the terms of the
[Creative Commons
Attribution 4.0 licence](#).

Any further distribution
of this work must
maintain attribution to
the author(s) and the title
of the work, journal
citation and DOI.



Li⁺ diffusion in crystalline lithium silicides: influence of intrinsic point defects

Christoph Kirsch¹ , Christian Dreßler² and Daniel Sebastiani^{1,*} ¹ Martin-Luther-University Halle-Wittenberg, Institute of Chemistry, Theoretical Chemistry, Von-Danckelmann-Platz 4, 06120 Halle (Saale), Germany² Ilmenau University of Technology, Theoretical Solid State Physics, Weimarer Straße 32, 98693 Ilmenau, Germany

* Author to whom any correspondence should be addressed.

E-mail: daniel.sebastiani@chemie.uni-halle.de**Keywords:** first principles molecular dynamics simulations, lithium diffusion, lithium-ion batteries, silicon anodes, intrinsic defectsSupplementary material for this article is available [online](#)

Abstract

Crystalline lithium silicides Li_xSi_y are a group of Zintl-like compounds, of which Li₁₅Si₄ is observed crystallizing in Si anodes after complete electrochemical lithiation. Here, Li diffusion in Li₁Si₁, Li₁₂Si₇, Li₁₃Si₄ and Li₁₅Si₄ is extensively studied by means of *ab initio* molecular dynamics simulations and nudged elastic band calculations considering various intrinsic point defects. Li interstitials are identified as the main vehicle of diffusion due to typically low formation and migration energies. They diffuse via an interstitialcy mechanism usually involving 2 or 3 atoms. Moreover, Frenkel defects are found to play a role in Li₁₂Si₇ and Li₁₃Si₄ only, as their formation energies are relatively high in Li₁Si₁ and Li₁₅Si₄. All investigated intrinsic defects have an impact on energy barriers of nearby as well as farther diffusion paths.

1. Introduction

Technological advances in fields such as renewable energy production and electric mobility demand high-performance energy storages, for example rechargeable batteries. While lithium-ion batteries (LIBs) are the established technology applied in portable electronic devices, they have also become the standard in present-day electric cars. Driven by growing research activities, a main objective is to further increase the batteries' energy density, with the potential to employ them in even larger-scale energy storage systems. The key to improving the energy density is searching for new electrode materials [1, 2].

One candidate anode material for future high-capacity LIBs is silicon. Exhibiting a gravimetric energy density of 3579 mAh g⁻¹ in its fully lithiated state Li₁₅Si₄ [3], Si is capable of storing about 10-fold the amount of Li compared to the most common anode material graphite (372 mAh g⁻¹ for LiC₆ [4]). Currently, the largest obstacle to the usage of silicon in LIBs is its substantially reduced cyclability compared to graphite due to mechanical failure of the Si anode. This is a result of considerable changes in structure and volume upon charging and discharging, e.g. Li₁₅Si₄ shows about 380% volume increase starting from crystalline silicon [3]. Graphite anodes do not suffer from this problem because lithium ions are reversibly intercalated between graphite layers during lithiation, which is accompanied by a volume expansion of only 13% (LiC₆) and rather small changes in structure. Thus, repeated lithiation and delithiation only cause a small capacity loss [4, 5]. A widely studied concept to handle the cycling issues of Si anodes is the utilization of silicon nanostructures and composite materials [3].

When a crystalline Si electrode is electrochemically lithiated under standard conditions, amorphous Li_xSi forms [6], which crystallizes to Li₁₅Si₄ at $x = 3.75$ and no further Li is inserted [7–9]. Delithiation of Li₁₅Si₄ leads to amorphous Li_xSi and eventually amorphous silicon [7, 8]. While Li₁₅Si₄ is the sole crystalline lithium silicide observed during cycling of a Si anode at room temperature, other Li_xSi_y compounds can be prepared at elevated temperatures. Syntheses of Li₁Si₁, Li₁₂Si₇, Li₇Si₃, Li₁₃Si₄, Li₁₅Si₄, Li_{4.11}Si₁, Li₂₁Si₅, Li₁₇Si₄ and

$\text{Li}_{22}\text{Si}_5$ have been reported [10–18]. Generally, crystalline lithium silicides are described as Zintl-like phases [19, 20].

It is important to understand Li mobility in such lithium–silicon compounds with well-defined structures, as the fundamental local diffusion mechanisms can possibly be transferred to more complex amorphous systems, in view of optimizing concepts for the design of actual Si anodes. Many properties of crystalline solids are heavily influenced by defects, including diffusivity. Therefore, intrinsic point defects, such as vacancies, self-interstitials, Frenkel and Schottky disorder, as well as extrinsic defects are commonly studied objects regarding diffusion in solids. Point defects give rise to various diffusion mechanisms, e.g. interstitial, interstitialcy and vacancy mechanisms. Additionally, non-defect mechanisms, like direct exchange, ring and chain-like mechanisms, can take place, but are usually higher in migration energy [21].

Li diffusivity has been studied experimentally in crystalline [22–26] and amorphous [27–29] lithium silicides. With regard to computational studies, diffusion of isolated Li ions has been investigated in crystalline [29–36] as well as amorphous [36] silicon by means of nudged elastic band (NEB) calculations. Furthermore, *ab initio* molecular dynamics (AIMDs) simulations have been carried out for the mixing of Li with crystalline [35, 37, 38] and amorphous [37] Si, and for lithium mobility in amorphous Li_xSi compounds [29, 39]. Crystalline Li_xSi_y have been studied by both AIMD simulations [40–43] and NEB calculations [38, 40–42, 44, 45].

While the before mentioned studies on Li migration in Li_xSi_y have all investigated defect-mediated diffusion, they typically focus on either a small selection of defects or compounds or both. Besides, most diffusion paths are hypothetical and have been constructed based on crystallographic considerations. This motivated the present study, which aims at systematically investigating intrinsic defects, namely Li interstitials, Li vacancies and a Schottky defect, in the four crystalline lithium silicides Li_1Si_1 , $\text{Li}_{12}\text{Si}_7$, $\text{Li}_{13}\text{Si}_4$ and $\text{Li}_{15}\text{Si}_4$. By a combination of AIMD simulations and NEB calculations, the arbitrariness in selection of the Li migration pathways is reduced.

2. Experimental section

2.1. Crystal structures

Crystallographic information on the investigated Li_xSi_y compounds is summarized in table 1. We focus on two crystals with high symmetry, tetragonal Li_1Si_1 [10] and cubic $\text{Li}_{15}\text{Si}_4$ [14] with one or two crystallographically distinct sites for Li and Si, and two less symmetric ones, orthorhombic $\text{Li}_{12}\text{Si}_7$ [11] and $\text{Li}_{13}\text{Si}_4$ [13] with 13 and 7 Li sites as well as 9 and 2 Si sites, respectively. With Li_xSi_y being Zintl-like phases [19, 20], different Si_n^{m-} polyanions are observed (Zintl ions): a network of threefold coordinated Si in Li_1Si_1 [10], planar Si_5 rings and planar Si_4 stars in $\text{Li}_{12}\text{Si}_7$ [11], Si_2 dumbbells and isolated Si in $\text{Li}_{13}\text{Si}_4$ [13], and only isolated Si in $\text{Li}_{15}\text{Si}_4$ [14]. Supercells of the crystal structures are illustrated in figure 1. Structures with labeled crystallographic Li sites as well as interstitial sites and metastable positions identified in this and a recent study [42] can be found in the supporting information, figures S1–S4. All structures in this work are visualized using either VESTA [46] or VMD [47].

2.2. Investigated systems with point defects

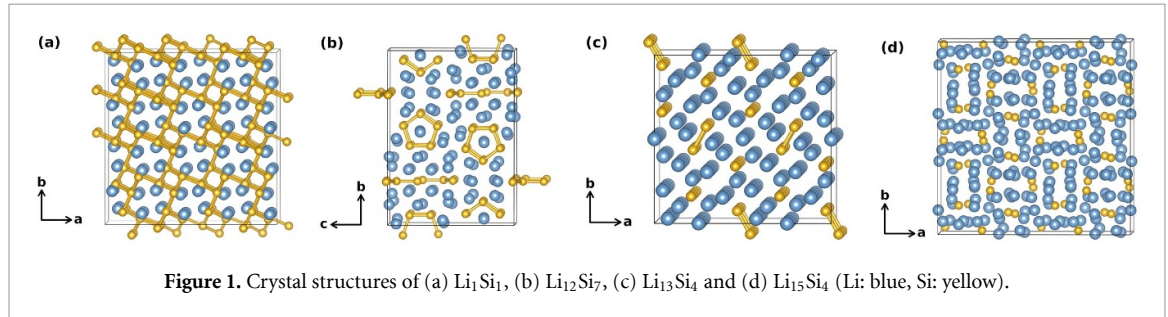
In order to study point defects in crystalline lithium silicides, we have constructed supercells from the crystal structures: $2 \times 2 \times 2$ for Li_1Si_1 , $1 \times 1 \times 1$ for $\text{Li}_{12}\text{Si}_7$, $2 \times 1 \times 3$ for $\text{Li}_{13}\text{Si}_4$ and $2 \times 2 \times 1$ for $\text{Li}_{15}\text{Si}_4$. For each compound, we have introduced defects into the supercell. Specifically, these were Li interstitials (Li_i^x), Li vacancies (v_{Li}^x) and one Schottky defect ($\text{v}_{\text{Li}}^x + \text{v}_{\text{Si}}^x$). Table 2 gives an overview of all investigated systems, which are given as Supplementary Data [48] (.xyz files) and are further characterized by lattice parameters in tables S2–S5 in the supporting information. The system listed first for each defect in table 2 was used as an initial structure for AIMD simulation. Subsequently, the defect could change its site through diffusion depending on the system. Interstitial sites were detected using a repulsive pair potential [49], geometrical considerations, and first principles MD results from this and a recent study [42]. Fractional coordinates of interstitial sites and metastable Li positions are given in table S1 in the supporting information.

2.3. Computational methods

All calculations were performed using density functional theory (DFT) [50, 51] as implemented in the program package CP2K [52, 53]. Within CP2K, the Quickstep code [53, 54] solves the Kohn–Sham equations [51] with the Gaussian plane wave method [55] applying a dual basis of atom-centered Gaussians for the orbitals and plane waves for the electronic density. A DZVP-MOLOPT-SR-GTH basis set [56] was used along with GTH-Perdew–Burke–Ernzerhof (PBE) pseudopotentials [57–59]. A plane-wave energy cutoff of 350 Ry and a relative cutoff of 40 Ry were chosen. Only the Γ point was sampled due to sufficiently large supercells. The exchange–correlation energy was described with the PBE functional [60, 61], and the

Table 1. Crystallographic information on lithium–silicon compounds studied in this work.

Compound	x/y	Space group	No. Li	No. Si	a (Å)	b (Å)	c (Å)	Reference
Li ₁ Si ₁	1.00	88 ($I4_1/a$)	16	16	9.354	9.354	5.746	[10]
Li ₁₂ Si ₇	1.71	62 ($Pnma$)	96	56	8.600	19.755	14.336	[11]
Li ₁₃ Si ₄	3.25	55 ($Pbam$)	26	8	7.949	15.125	4.466	[13]
Li ₁₅ Si ₄	3.75	220 ($I\bar{4}3d$)	60	16	10.687	10.687	10.687	[14]

**Figure 1.** Crystal structures of (a) Li₁Si₁, (b) Li₁₂Si₇, (c) Li₁₃Si₄ and (d) Li₁₅Si₄ (Li: blue, Si: yellow).**Table 2.** Data on studied systems containing point defects.

Compound	Defect	System	Compound	Defect	System
Li ₁ Si ₁	Li _i [×]	Li @ Int1 Li @ Int2	Li ₁₃ Si ₄	Li _i [×]	Li @ Li2 ^(a) Li @ Li1/Li2 ^(b)
	v _{Li} [×]	v @ Li1		v _{Li} [×]	v @ Li1/Li2 ^(c)
	v _{Li} [×] + v _{Si} [×]	v @ Li1 + v @ Si1			v @ Li1
Li ₁₂ Si ₇	Li _i [×]	Li @ Int1 Li @ Int2	Li ₁₅ Si ₄	Li _i [×]	Li @ Int
	v _{Li} [×]	v @ Li9 v @ Li8		v _{Li} [×]	v @ Li1 v @ Li2

^(a) Split interstitial/dumbbell interstitial, 2 Li atoms occupying Li2.

^(b) Crowdion-like interstitial, 5 Li atoms occupying 2 × Li1 and 2 × Li2.

^(c) 4 Li atoms occupying 4 × Li1 and 1 × Li2.

DFT-D3 method was employed for dispersion correction [62]. Broyden mixing [63] with $\alpha = 0.2$ and Fermi–Dirac smearing [64] with an electronic temperature of 600 K were used for a self-consistent field convergence accuracy of 10^{-6} . For all calculations, periodic boundary conditions were applied and the total charge of the systems was neutral.

To set up the systems described in section 2.2 for AIMD simulations and NEB calculations, lattice parameters and atomic coordinates had to be relaxed. In a first step, lattice constants and atomic positions of both defect-free and defect-containing systems were fully relaxed at zero temperature and 1 atm pressure. The computed lattice constants of the systems with defects were scaled with a correction factor obtained from the ratio of the experimental (see table 1) versus computed lattice constants for the defect-free systems. This correction can be seen as an approximation for the thermal expansion as well as for systematic computational errors in the cell optimization. In analogy to this, the lattice constants for the defect-free crystals were equally scaled to the corresponding experimental values. Finally, atomic coordinates were fully relaxed within fixed corrected lattice parameters for each system. All cell and geometry optimizations were carried out using a Broyden–Fletcher–Goldfarb–Shanno minimizer [65–68].

AIMDs simulations were performed with a time step of 1 fs in a canonical ensemble (NVT) at 500 K (Li₁₂Si₇, Li₁₃Si₄) or 800 K (Li₁Si₁, Li₁₅Si₄) controlled by a Nosé–Hoover chain thermostat [69, 70]. The relaxed systems were equilibrated for 1 ps applying massive thermostating with a time constant of $\tau = 10$ fs, followed by 1 ps with $\tau = 100$ fs. Then, 100 ps of trajectory with a global thermostat and $\tau = 100$ fs were produced for analysis.

Li diffusion pathways observed in the AIMD simulations were mapped with climbing image [71] NEB [72–75] (CI-NEB) calculations using 16 replicas including initial and final structure with fully relaxed atomic positions, that were fixed in the NEB calculation.

Lattice parameters and atomic coordinates of all defect-free as well as defect-containing structures were re-optimized with the following adjusted DFT parameters to calculate defect formation energies: no

dispersion correction, TZVP-MOLOPT-GTH (Si) and TZVP-MOLOPT-SR-GTH (Li) basis sets, and a Monkhorst–Pack scheme [76] k -point sampling for Brillouin zone integration (for used meshes see supporting information, table S6). Crystal structures of elemental Li and Si were fully relaxed accordingly. Defect formation energies were then calculated from the following formula [77]:

$$E_{\text{form}}(\text{defect}) = E(\text{defect}) - E(\text{bulk}) - \sum_i n_i \mu_i. \quad (1)$$

$E(\text{defect})$ and $E(\text{bulk})$ are the energies of the defect-containing and defect-free systems, respectively, n_i are the numbers of atoms of element i added or removed to transform the latter into the former system and μ_i are the chemical potentials of one respective atom, which are approximated as the energies of one atom in the elemental crystal structure.

Elastic constants were computed following an established stress–strain methodology from the literature [78], that is described in section S1.1 in the supporting information. Diffusion coefficients were determined via the mean square displacements (MSDs), see section S1.2 in the supporting information for details. Formation energies of the compounds were calculated according to section S1.3 in the supporting information.

3. Results and discussion

3.1. Interstitial Li atoms

Li diffusion coefficients in Li_1Si_1 , $\text{Li}_{12}\text{Si}_7$, $\text{Li}_{13}\text{Si}_4$ and $\text{Li}_{15}\text{Si}_4$ systems containing intrinsic points defects (see section 2.2) were calculated from AIMD simulations according to equation (S5) and are given in table 3. Corresponding MSDs are shown in the supporting information, figure S5. Results of defect-free systems are taken from [42] for comparison. $\text{Li}_{12}\text{Si}_7$ and $\text{Li}_{13}\text{Si}_4$ were simulated at 500 K, Li_1Si_1 and $\text{Li}_{15}\text{Si}_4$ at 800 K. According to Braga *et al* Li_1Si_1 , $\text{Li}_{12}\text{Si}_7$ and $\text{Li}_{13}\text{Si}_4$ are stable at these temperatures, while $\text{Li}_{15}\text{Si}_4$ is narrowly stable around room temperature only [79]. However, decomposition was not observed in any trajectory, due to fixed cell parameters and only 100 ps simulation time. Chevrier *et al* obtained Li partial atomic charges of approximately $+0.73e$ in all crystalline Li_xSi_y , from Bader charge analysis [20]. Therefore, Li can be assumed to be cationic in these compounds and to diffuse as Li^+ as well.

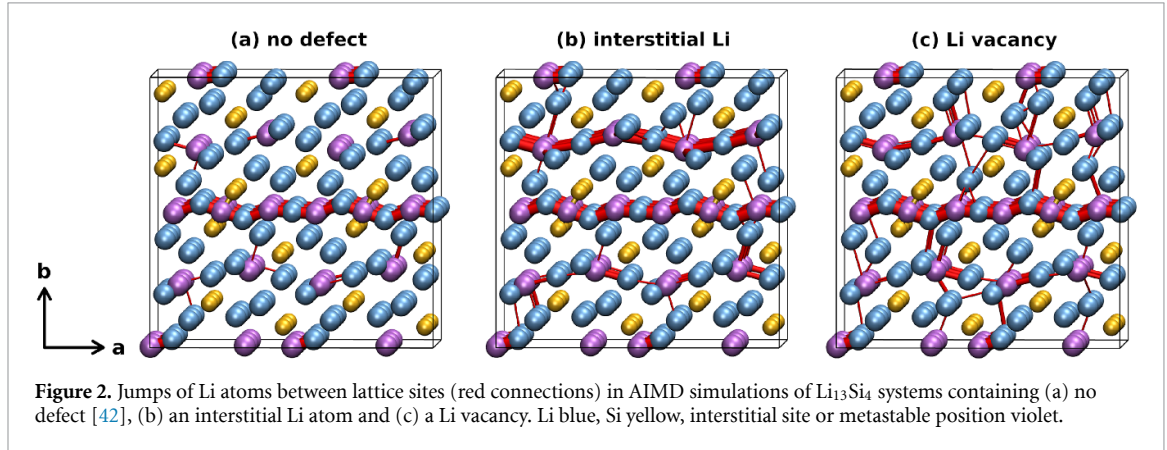
Experimentally, Li diffusivities were measured to be $\approx 4 \cdot 10^{-7} \text{ cm}^2 \text{ s}^{-1}$ at 573 K [26] and $5 \cdot 10^{-7} \text{ cm}^2 \text{ s}^{-1}$ at 688 K [22] in $\text{Li}_{12}\text{Si}_7$, and $4 \cdot 10^{-7} \text{ cm}^2 \text{ s}^{-1}$ at 688 K [22] in $\text{Li}_{13}\text{Si}_4$. The values presented in this study are between a factor of 2 and 10 higher, which can at least partially be attributed to supercell size as discussed in [42]. Gruber *et al* used a smaller cell for $\text{Li}_{13}\text{Si}_4$ and obtained an even higher D_{Li} of $\approx 300 \cdot 10^{-7} \text{ cm}^2 \text{ s}^{-1}$ at 500 K [41]. For both computational and experimental values, $\text{Li}_{12}\text{Si}_7$ and $\text{Li}_{13}\text{Si}_4$ are fast Li ionic conductors. The same applies to $\text{Li}_{15}\text{Si}_4$ in this study if interstitial Li atoms are considered. No diffusion is observed in Li_1Si_1 . The exclusion of Li interstitials has no effect on the diffusivity in Li_1Si_1 , $\text{Li}_{12}\text{Si}_7$ and $\text{Li}_{13}\text{Si}_4$, but substantially reduces D_{Li} in $\text{Li}_{15}\text{Si}_4$. Note that here the term ‘defect’ refers to changing the numbers of atoms of certain elements in the system, i.e. all structures with the original stoichiometric atom numbers are considered as ‘defect-free’ systems. Because diffusion takes place via low-energy migration paths mediated by Frenkel disorder in $\text{Li}_{12}\text{Si}_7$ and by a transition to a metastable structure in $\text{Li}_{13}\text{Si}_4$, these compounds exhibit high Li diffusivities even in the defect-free systems. Therefore, we conclude that D_{Li} can increase by introduction of an interstitial Li atom, if no defect-free diffusion is possible ($\text{Li}_{15}\text{Si}_4$), but is unaltered if defect-free diffusion is already high ($\text{Li}_{12}\text{Si}_7$, $\text{Li}_{13}\text{Si}_4$) or if interstitial Li diffusion is high in energy (Li_1Si_1 , for discussion of migration energies see below). Formation energies of Li_1Si_1 , $\text{Li}_{12}\text{Si}_7$, $\text{Li}_{13}\text{Si}_4$ and $\text{Li}_{15}\text{Si}_4$ were calculated according to equation (S6). The respective values are -0.18 , -0.23 , -0.24 , and -0.22 eV/atom. We point out that these values correlate with the defect-free Li diffusivities: the more thermodynamically stable the compound, the higher the diffusion coefficient. The reason for this correlation is not obvious, but it is also important to note that the data set, consisting of only four points, is very limited. Regarding (an)isotropy of diffusion, we report spatially resolved D_{Li} in table S7 in the supporting information. While anisotropy changes only slightly in $\text{Li}_{12}\text{Si}_7$ with interstitial Li, in $\text{Li}_{13}\text{Si}_4$ new diffusion paths result in anisotropic three-dimensional instead of highly anisotropic one-dimensional diffusion in the defect-free system. In $\text{Li}_{15}\text{Si}_4$ diffusion is isotropic, as expected for a cubic crystal structure.

A protocol to map overall diffusivities to a more atomistic picture of atom jumps between lattice sites was described in detail in [42] and employed here. The results are depicted in figures 2 ($\text{Li}_{13}\text{Si}_4$) and S6–S8 (Li_1Si_1 , $\text{Li}_{12}\text{Si}_7$, $\text{Li}_{15}\text{Si}_4$). Relaxed atomic coordinates of a defect-free system define the basic lattice for a given compound, and jumps between lattice sites in our MD trajectories are counted and visualized by red lines for each pair of lattice sites. The line thickness is scaled logarithmically according to the jump frequency. Since it was shown that interstitial sites and metastable positions are necessary for a reliable jump detection [42], their coordinates are also considered as lattice sites.

Table 3. Li diffusivities D_{Li} / ($10^{-3} \text{ \AA}^2 \text{ ps}^{-1} = 10^{-7} \text{ cm}^2 \text{ s}^{-1}$) in crystalline Li_xSi_y systems containing intrinsic defects, calculated from AIMD simulations, $\text{Li}_{12}\text{Si}_7$ and $\text{Li}_{13}\text{Si}_4$ at 500 K, Li_1Si_1 and $\text{Li}_{15}\text{Si}_4$ at 800 K, defect-free results from [42].

Compound	No defect [42]	Li_i^\times	v_{Li}^\times	$v_{\text{Li}}^\times + v_{\text{Si}}^\times$
Li_1Si_1	0.0	0.0	1.0	0.7
$\text{Li}_{12}\text{Si}_7$	11.6	11.4	10.5	— ^a
$\text{Li}_{13}\text{Si}_4$	39.5	46.3	21.2	— ^a
$\text{Li}_{15}\text{Si}_4$	0.2	18.6	7.5	— ^a

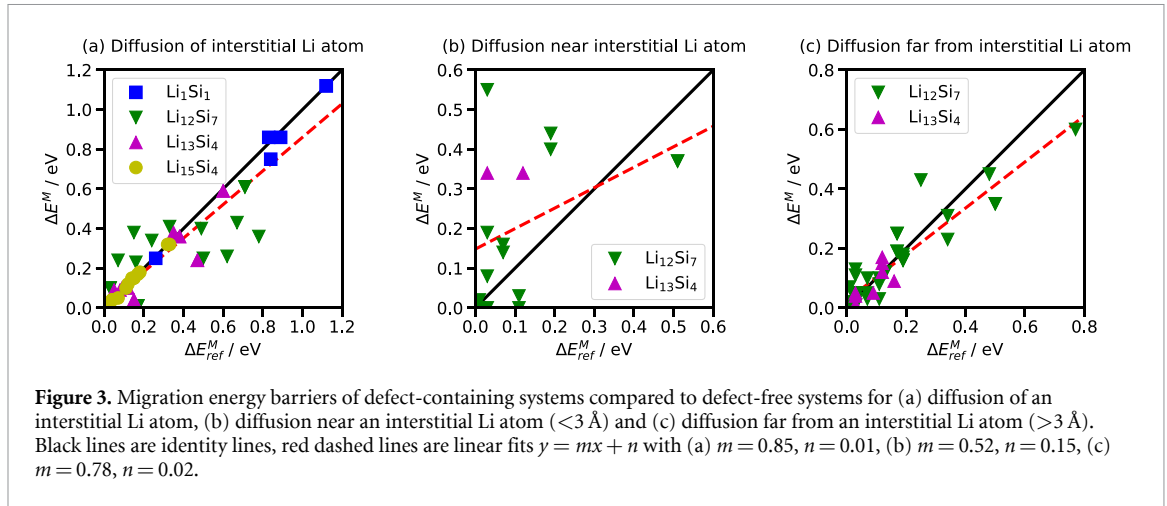
^a Not studied.



For $\text{Li}_{12}\text{Si}_7$ and $\text{Li}_{13}\text{Si}_4$, the contributions of individual lattice sites to defect-free Li diffusion were discussed in detail in [42]. Here, the focus is only on describing the differences that arise from an interstitial Li atom. In Li_1Si_1 and $\text{Li}_{15}\text{Si}_4$, defect-free diffusion is close to zero. Detected jumps in figures S6(a) and S8(a) are an artifact and can be ascribed to thermal vibrations. Regarding the systems with an interstitial Li atom, no Li jumps are detected for Li_1Si_1 , while many jumps can be observed in $\text{Li}_{12}\text{Si}_7$, $\text{Li}_{13}\text{Si}_4$ and $\text{Li}_{15}\text{Si}_4$. Comparison with the defect-free systems shows no change in the total jump numbers for Li_1Si_1 and $\text{Li}_{12}\text{Si}_7$, a slight increase for $\text{Li}_{13}\text{Si}_4$ and a larger one for $\text{Li}_{15}\text{Si}_4$. These results are in accordance with the Li diffusivities discussed above. In both $\text{Li}_{12}\text{Si}_7$ and $\text{Li}_{13}\text{Si}_4$, new connections between lattice sites are detected in the upper half of the depicted systems, which is where the interstitial Li atom was located in the trajectories, respectively. For $\text{Li}_{12}\text{Si}_7$, these new connections are for example Li5-Li7, Li5-Li11, Li7-Li12 and Li11-Li13, while other connections vary in frequency. Overall, the jumps reflect anisotropic diffusion as mentioned above. In $\text{Li}_{13}\text{Si}_4$, in addition to the unaltered prevalent jump pattern involving Li1, Li2, M1 and M2 known from the defect-free system, many jumps are observed between Li6 and Int in x -direction and between Li3 and Int in z -direction. This directly maps the change in diffusion anisotropy discussed for D_{Li} to an atomistic picture of involved lattice sites, explaining the new component of Li diffusivity in z -direction. For $\text{Li}_{15}\text{Si}_4$, connections are detected between Li1-Li1, Li1-Li2, Li1-Int, Li2-Int and Int-Int, causing an isotropic picture of diffusion.

NEB calculations were performed on migration pathways observed in the AIMD simulations or constructed theoretically in order to obtain an even more atomistic picture of diffusion. The compounds' crystal structures along with crystallographic Li and Si sites, as well as interstitial sites and metastable positions for Li were described in sections 2.1 and 2.2. All investigated Li_xSi_y exhibit one or two crystallographically distinct interstitial Li sites, but $\text{Li}_{13}\text{Si}_4$ can additionally accommodate interstitial Li atoms as split interstitials and crowdion-like interstitials. The studied diffusion paths for each system are analysed in terms of involved sites, diffusion mechanisms and migration energies in tables S9, S13, S16 and S19 in the supporting information. Additionally, the fully relaxed pathways are given as Supplementary Data [48] (.xyz files) together with the respective energy profiles (.txt files). The lowest-energy paths for interstitial Li diffusion in each compound are also illustrated in figures S9 (a), S10 (a), S11 (a) and S12 (a). All paths are numbered consecutively for distinction, and to compare the same unique path within different systems. In the systems containing defects, a path number appended by '_def' indicates that the defect itself diffuses, '_near' refers to a path with at least one of the diffusing atoms in vicinity ($<3 \text{ \AA}$) to the defect, and '_far' means that the path takes place with a distance of $>3 \text{ \AA}$ to the defect.

We found that interstitial Li diffusion pathways follow interstitialcy—also called indirect interstitial—rather than direct interstitial mechanisms in the four studied compounds. The migration energy barriers for observed interstitialcy paths vary between 0.25–0.86 eV in Li_1Si_1 , 0.01–0.25 eV in $\text{Li}_{12}\text{Si}_7$, 0.03–0.38 eV in $\text{Li}_{13}\text{Si}_4$ and 0.00–0.32 eV in $\text{Li}_{15}\text{Si}_4$, respectively. These low barriers in $\text{Li}_{12}\text{Si}_7$, $\text{Li}_{13}\text{Si}_4$ and $\text{Li}_{15}\text{Si}_4$ cause high



diffusivities as discussed above. Most typically, 2 or 3 Li atoms migrate simultaneously. Whereas direct interstitial diffusion is not observed in Li_1Si_1 , $\text{Li}_{12}\text{Si}_7$ and $\text{Li}_{13}\text{Si}_4$, which is consistent with minimum migration barriers of 0.69 and 0.41 eV for constructed paths in Li_1Si_1 and $\text{Li}_{12}\text{Si}_7$, a migration energy of only 0.04 eV would make this mechanism possible in $\text{Li}_{15}\text{Si}_4$. Few direct jumps between two interstitial sites have also been detected by the protocol described above. However, when relaxing every 1000th snapshot of the $\text{Li}_{15}\text{Si}_4$ trajectory and tracing atom coordinate changes between the snapshots, these direct interstitial jumps could not be identified, and thus might be detection errors of our protocol. Overall, direct interstitial diffusion could be possible in $\text{Li}_{15}\text{Si}_4$, but is observed significantly less frequently than interstitialcy diffusion.

Considering Li migration via interstitialcy mechanisms in more detail, no low-energy path is found in Li_1Si_1 . In $\text{Li}_{12}\text{Si}_7$, especially path (40)_def with the jump pattern $\text{Li}_{\text{Int}1} \rightarrow \text{Li}_{12} \rightarrow \text{Int}1$ and only 0.01 eV migration energy adds to the low-energy paths already discussed in [42], that originate from Frenkel defects. In $\text{Li}_{13}\text{Si}_4$, the prevalent low-energy path from the defect-free structure [42], here path (44), is supplemented by paths (49)_def ($\text{Li}_{\text{Int}} \rightarrow \text{Li}_3 \rightarrow \text{Int}$) and (50)_def ($\text{Li}_{\text{Int}} \rightarrow \text{Li}_6 \rightarrow \text{Int}$) with energy barriers of 0.09 and 0.10 eV, respectively. Path (49)_def causes the diffusivity component in z -direction. For $\text{Li}_{15}\text{Si}_4$, paths (61)_def, (62)_def, (63)_def and (65)_def are comparatively low in energy, making interstitialcy mechanisms with 2, 3 or 4 involved atoms equally important for interstitial Li diffusion.

In order to investigate the importance of interstitial defects, we have correlated the NEB migration barriers computed for Li_xSi_y systems *with* interstitial Li atoms to the corresponding barriers of the same paths in systems *without* Li interstitials. In figure 3, this is done for (a) diffusion of the defect itself, i.e. compared to an interstitial Li atom from a Frenkel defect in an otherwise defect-free system, (b) diffusion near the defect ($<3 \text{ \AA}$) compared to a path in absence of it and (c) diffusion far from the defect ($>3 \text{ \AA}$) compared to a path without it. As a guide to the eye, linear regressions are performed on these energy barriers to identify trends.

In figure 3(a), it is evident that for Li_1Si_1 and especially for $\text{Li}_{15}\text{Si}_4$ the data points are close to or on the identity line, while for $\text{Li}_{12}\text{Si}_7$ and $\text{Li}_{13}\text{Si}_4$ they are not. Considering differences between defect formation energies of a Frenkel defect and the sum of an isolated Li interstitial and an isolated Li vacancy (see table 5), these are -0.11 eV (Int1) and -0.17 eV (Int2) for Li_1Si_1 , -0.17 eV (Int1) and 0.03 eV (Int2) for $\text{Li}_{12}\text{Si}_7$, -0.18 eV (Int) for $\text{Li}_{13}\text{Si}_4$ and 0.01 eV (Int) for $\text{Li}_{15}\text{Si}_4$. These suggest that interstitial Li atom and Li vacancy of a Frenkel defect are considerably more separated in $\text{Li}_{15}\text{Si}_4$ than they are in Li_1Si_1 , $\text{Li}_{12}\text{Si}_7$ and $\text{Li}_{13}\text{Si}_4$, because negative values can be understood as stabilisation via electrostatic interaction. Subsequent migration of the Frenkel interstitial Li atom in $\text{Li}_{15}\text{Si}_4$ is then relatively unaffected by interactions with the Li vacancy, it diffuses like a separate interstitial Li atom, causing the points to be on the identity line. For $\text{Li}_{12}\text{Si}_7$ and $\text{Li}_{13}\text{Si}_4$, it appears that small migration energies of a Frenkel interstitial Li, possibly favoured by electrostatic interaction, tend to increase without the vacancy, whereas larger migration barriers tend to decrease. Note that the spread of ΔE^M is rather large for a given ΔE_{ref}^M , meaning that paths behave very differently when comparing separate interstitial Li atoms with those from Frenkel defects. Nevertheless, the linear regression reveals on average 15% smaller migration barriers for separate interstitial Li atoms. In figure 3 (b), the influence of interstitial Li atoms on other Li atoms diffusing by them within 3 \AA is illustrated. Most of the investigated paths increase in energy, some drastically up to $+0.5 \text{ eV}$, and only few decrease. The spread of data is too large to give a meaningful linear fit, but it can be concluded that interstitial Li atoms clearly move the potential to block diffusion pathways. Figure 3(c) shows the potential impact of interstitial Li atoms on paths with a distance of more than 3 \AA to the defect. The data points are on the identity line with medium spread, showing no large influence of the defect. A linear regression gives an average 22% decrease in

Table 4. Voigt averages of bulk moduli K_V / GPa and shear moduli G_V / GPa for crystalline Li_xSi_y systems containing intrinsic defects as well as no defect.

Compound	System	K_V	G_V	Compound	System	K_V	G_V
No defect							
Li_1Si_1		52.9	38.9	$\text{Li}_{13}\text{Si}_4$		32.7	29.3
$\text{Li}_{12}\text{Si}_7$		37.4	33.9	$\text{Li}_{15}\text{Si}_4$		30.2	23.1
Li_i^\times							
Li_1Si_1	Li @ Int1	52.8	38.7	$\text{Li}_{13}\text{Si}_4$	Li @ Li2 ^(a)	32.0	29.2
	Li @ Int2	52.7	38.4		Li @ Li1/Li2 ^(b)	32.6	29.5
$\text{Li}_{12}\text{Si}_7$	Li @ Int1	36.4	33.8		Li @ Int	32.6	29.4
	Li @ Int2	36.7	32.7	$\text{Li}_{15}\text{Si}_4$	Li @ Int	29.9	23.0
$\text{v}_{\text{Li}}^\times$							
Li_1Si_1	v @ Li1	52.7	38.1	$\text{Li}_{13}\text{Si}_4$	v @ Li1/Li2 ^(c)	32.3	29.1
$\text{Li}_{12}\text{Si}_7$	v @ Li8	36.1	32.9		v @ Li1	32.3	29.2
	v @ Li9	35.5	32.6	$\text{Li}_{15}\text{Si}_4$	v @ Li1	29.9	22.6
					v @ Li2	29.8	22.3
$\text{v}_{\text{Li}}^\times + \text{v}_{\text{Si}}^\times$							
Li_1Si_1	v @ Li1, v @ Si1	51.1	36.3				

^(a) Split interstitial/dumbbell interstitial, 2 Li atoms occupying Li2.

^(b) Crowdion-like interstitial, 5 Li atoms occupying $2 \times \text{Li1}$ and $2 \times \text{Li2}$.

^(c) 4 Li atoms occupying $4 \times \text{Li1}$ and $1 \times \text{Li2}$.

migration energy due to the defect, revealing a potential small effect, which, however, is only really observed for $\text{Li}_{12}\text{Si}_7$. This is further discussed in connection with elastic properties.

Elastic constants of all systems were computed according to section 2.3, from which bulk and shear moduli were calculated and are given in table 4. Generally, bulk and shear moduli decrease with increasing Li content and weakening Si–Si connectivity, meaning that crystalline lithium silicides become softer in the order Li_1Si_1 , $\text{Li}_{12}\text{Si}_7$, $\text{Li}_{13}\text{Si}_4$ and $\text{Li}_{15}\text{Si}_4$. Li_1Si_1 is significantly stiffer than the other three due to the network of Si–Si bonds. While the elastic properties alone do not correlate with the Li diffusivity in the compounds, softening or hardening of a crystal lattice could influence migration barriers, since atomic jumps in solids require pushing aside other atoms and therefore straining the lattice. For interstitial Li atoms, all of the investigated systems exhibit a slight decrease in K_V ($-0.1 \dots -1.0$ GPa) and most of them also in G_V ($+0.2 \dots -1.2$ GPa), indicating softening compared to defect-free systems. This fits to the results presented in figure 3(c), that show a small decrease in migration energy barriers, which might now be interpreted as a consequence of lattice softening. It is only reasonable to consider the paths in larger distance to the defect here, since these are not affected locally by it, and the elastic moduli are calculated for the entire system and therefore non-local as well.

Apart from the migration energy barriers of defects, it is equally important to consider their concentrations in order to evaluate whether they contribute to diffusion. Concentrations of defects are determined by their formation energies: higher E_{form} result in lower concentrations and, consequently, lower diffusivity for a given diffusion barrier, and vice versa. Defect formation energies were calculated according to section 2.3 and are given in table 5. Interstitial Li atom formation energies are generally low in all considered compounds making Li interstitials a very probable intrinsic defect. For the regular interstitial sites in $\text{Li}_{12}\text{Si}_7$ and $\text{Li}_{13}\text{Si}_4$, E_{form} is even negative, indicating unhindered Li incorporation when in contact with a Li reservoir. Formation energies of regular interstitials in Li_1Si_1 and $\text{Li}_{15}\text{Si}_4$ as well as for split and crowdion-like interstitials in $\text{Li}_{13}\text{Si}_4$ are between 0.22 eV and 0.29 eV and therefore also very low, with Int1 in Li_1Si_1 being the only exception. Equilibrium interstitial site fractions in a NVT ensemble are given by $[\text{Li}_i] = g \exp(-\frac{E_{\text{form}}}{k_B T})$. Assuming the geometric factor g to be 1, which is valid for regular interstitials, and approximating F_{form}^* by E_{form} neglecting entropic contributions, Li interstitial concentrations can be estimated by the Boltzmann factor $\exp(-\frac{E_{\text{form}}}{k_B T})$, giving $[\text{Li}_i] \approx 10^{-4}$ to 10^{-5} for formation energies between 0.22 eV and 0.29 eV at room temperature.

Table 5. Defect formation energies E_{form} / eV for crystalline Li_xSi_y systems containing intrinsic defects.

Compound	System	E_{form}	Compound	System	E_{form}
$\text{Li}_i^\times + \text{v}_{\text{Li}}^\times$					
Li_1Si_1	Li @ Int1, v @ Li1	1.61	$\text{Li}_{13}\text{Si}_4$	Li @ Int, v @ Li1	0.28
	Li @ Int2, v @ Li1	1.11			
$\text{Li}_{12}\text{Si}_7$	Li @ Int1, v @ Li8	0.29	$\text{Li}_{15}\text{Si}_4$	Li @ Int, v @ Li1	1.57
	Li @ Int2, v @ Li8	0.58			
Li_i^\times					
Li_1Si_1	Li @ Int1	0.69	$\text{Li}_{13}\text{Si}_4$	Li @ Li2 ^(a)	0.28
	Li @ Int2	0.25		Li @ Li1/Li2 ^(b)	0.29
$\text{Li}_{12}\text{Si}_7$	Li @ Int1	-0.21	$\text{Li}_{15}\text{Si}_4$	Li @ Int	-0.29
	Li @ Int2	-0.12		Li @ Int	0.22
$\text{v}_{\text{Li}}^\times$					
Li_1Si_1	v @ Li1	1.03	$\text{Li}_{13}\text{Si}_4$	v @ Li1/Li2 ^(c)	0.78
$\text{Li}_{12}\text{Si}_7$	v @ Li8	0.67		v @ Li1	0.75
	v @ Li9	0.80	$\text{Li}_{15}\text{Si}_4$	v @ Li1	1.34
				v @ Li2	1.54
$\text{v}_{\text{Li}}^\times + \text{v}_{\text{Si}}^\times$					
Li_1Si_1	v @ Li1, v @ Si1	2.69			

^(a) Split interstitial/dumbbell interstitial, 2 Li atoms occupying Li2.

^(b) Crowdion-like interstitial, 5 Li atoms occupying $2 \times \text{Li1}$ and $2 \times \text{Li2}$.

^(c) 4 Li atoms occupying $4 \times \text{Li1}$ and $1 \times \text{Li2}$.

In conclusion, Li diffusivity in crystalline Li_xSi_y can increase or remain relatively uninfluenced by interstitial Li atoms, and diffusion (an)isotropy can be altered. Li interstitials are found to migrate via interstitialcy diffusion mechanisms involving 2 or 3 atoms much more likely than via interstitial mechanisms. Generally, migration energy barriers are on average 15% smaller compared to Li interstitials created by Frenkel defects. Interstitial Li atoms have a local effect by increasing energy barriers for paths in vicinity by up to 0.5 eV, and a potential non-local effect by decreasing migration energies on average by 22% via lattice softening. Moreover, Li interstitial formation is very likely in all Li_xSi_y due to low formation energies of typically below 0.3 eV. From a perspective of the individual compounds, $\text{Li}_{15}\text{Si}_4$ becomes a fast ionic conductor with interstitial Li atoms, making it comparable to $\text{Li}_{12}\text{Si}_7$ and $\text{Li}_{13}\text{Si}_4$, that both exhibit high diffusivities even in the stoichiometric systems. For all three compounds, close-to-zero energy migration paths exist for interstitialcy diffusion, whereas migration barriers in Li_1Si_1 are significantly larger, hindering fast Li diffusion in this compound.

3.2. Li vacancies

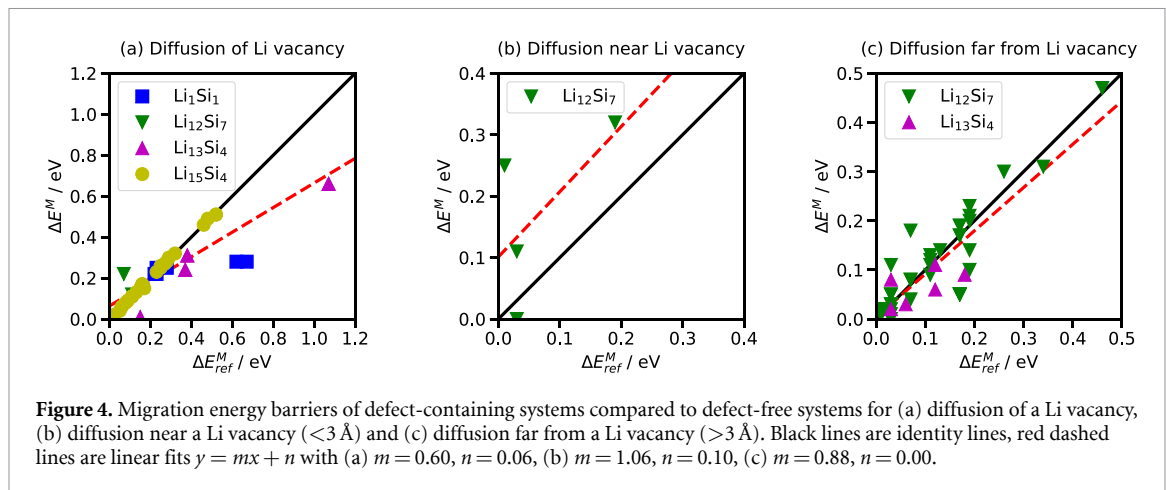
Li diffusivities in Li_1Si_1 , $\text{Li}_{12}\text{Si}_7$, $\text{Li}_{13}\text{Si}_4$ and $\text{Li}_{15}\text{Si}_4$ containing a Li vacancy are shown in table 3. Li_1Si_1 exhibits low, but non-zero diffusion, $\text{Li}_{12}\text{Si}_7$ and $\text{Li}_{13}\text{Si}_4$ remain very good ion conductors, and D_{Li} in $\text{Li}_{15}\text{Si}_4$ is in between. In comparison with the defect-free systems, Li diffusion coefficients increase for Li_1Si_1 and $\text{Li}_{15}\text{Si}_4$, which are both compounds with zero defect-free diffusion. In $\text{Li}_{12}\text{Si}_7$, diffusivity is unchanged, while in $\text{Li}_{13}\text{Si}_4$ it is even halved. Li_1Si_1 is the only compound studied here with higher vacancy- than interstitial-mediated Li diffusion, whereas it is relatively constant in $\text{Li}_{12}\text{Si}_7$ and significantly lower in $\text{Li}_{13}\text{Si}_4$ and $\text{Li}_{15}\text{Si}_4$. (An)isotropy of diffusion is discussed by means of values for D_x , D_y and D_z presented in table S7 in the supporting information. Li diffusion in Li_1Si_1 shows a $D_x = D_y \neq D_z$ behaviour expected for a tetragonal crystal structure. In orthorhombic $\text{Li}_{12}\text{Si}_7$, diffusion is anisotropic in all systems, but the ratio of D_x , D_y and D_z is different in the defect-free and both of the so far discussed defect-containing systems, indicating that each defect can alter anisotropy uniquely. In orthorhombic $\text{Li}_{13}\text{Si}_4$, D_x is by far the largest component in all systems, but as already observed for the Li interstitial, diffusion is not one-dimensional as in the defect-free system, but rather three-dimensional. Anisotropy is higher with the Li vacancy than with the interstitial Li atom, because D_z is substantially smaller. Diffusion in cubic $\text{Li}_{15}\text{Si}_4$ is isotropic for both Li vacancy and Li interstitial.

Atom jumps between lattice sites were analysed and are illustrated in figure 2 for $\text{Li}_{13}\text{Si}_4$ and S6-S8 for Li_1Si_1 , $\text{Li}_{12}\text{Si}_7$ and $\text{Li}_{15}\text{Si}_4$. No jumps apart from detection errors are depicted in Li_1Si_1 due to an applied threshold for a minimum number of jumps required. In $\text{Li}_{12}\text{Si}_7$, many jumps are observed reflecting anisotropic diffusion discussed above. Connections between lattice sites appear very similar with a Li vacancy, that is found in the upper half of the depicted system in the trajectory, compared to the defect-free system. New connections are merely observed between Li5 and Li12. Atom jumps observed uniquely with a Li interstitial are missing with a Li vacancy again. In $\text{Li}_{13}\text{Si}_4$, the large number of jumps involving Li1, Li2, M1 and M2 causing high diffusivity in x -direction is prevalent for all studied systems. It was discussed in section 3.1 that additional connections appear with an interstitial Li atom. This is the case with a Li vacancy as well, causing components of D_{Li} in y - and z -direction. It is visible that these connections differ in both systems, for example, there is no large number of jumps involving Li3 or Li6 with a Li vacancy, explaining lower D_x and D_z . In $\text{Li}_{15}\text{Si}_4$, many isotropic jumps are detected between Li1-Li1, Li1-Li2 and Li1-Int, but the total number of jumps is lower than with an interstitial Li atom, which is in accordance with calculated Li diffusivities.

In the AIMD simulations of the investigated crystalline lithium silicides, Li vacancies were initially introduced into the crystal structure according to table 2, and for a major part of the trajectories they were observed on Li1 in Li_1Si_1 , on Li8 or Li9 in $\text{Li}_{12}\text{Si}_7$, on Li1 or distributed over rows of Li1 and Li2 in $\text{Li}_{13}\text{Si}_4$ and on Li1 or Li2 in $\text{Li}_{15}\text{Si}_4$. Migration pathways of the vacancies between these lattice sites were computed using NEB calculations, along with other observed paths. Detailed results are given in tables S10, S14, S17 and S20 as well as figures S9 (b), S10 (b), S11 (b) and S12 (b) in the supporting information and as Supplementary Data [48]. In $\text{Li}_{12}\text{Si}_7$, a vacancy on Li8 or Li9 leads to occupation of the adjacent metastable position M1 or M2 by the second adjacent Li8 or Li9, respectively. In $\text{Li}_{13}\text{Si}_4$, a vacancy on Li1 drives the second adjacent Li1 onto M1, and a vacancy on Li2 becomes distributed over 5 lattice sites by $2 \times$ Li1 moving to $2 \times$ M2 adjacent to the Li2 vacancy and $2 \times$ Li1 moving to $2 \times$ M1 adjacent to the 2 Li1 vacancies created before. Thus, vacancies in $\text{Li}_{12}\text{Si}_7$ and $\text{Li}_{13}\text{Si}_4$ are usually distributed over at least two lattice sites by occupation of metastable Li positions, in which a Li atom is placed between two regular lattice sites, whereas in Li_1Si_1 and $\text{Li}_{15}\text{Si}_4$ regular single-site vacancies are found.

Consequently, Li vacancy migration follows a standard vacancy mechanism with single-atom jumps in Li_1Si_1 and $\text{Li}_{15}\text{Si}_4$. In contrast, at least 3 atoms move collectively in $\text{Li}_{12}\text{Si}_7$ as well as $\text{Li}_{13}\text{Si}_4$, and vacancy jumps are coupled to (de)occupation of metastable Li sites, which is a result of the distributed nature of Li vacancies in these two compounds as discussed above. Calculated migration energies of isolated Li vacancies are 0.22–0.28 eV in Li_1Si_1 , 0.05–0.32 eV in $\text{Li}_{12}\text{Si}_7$, 0.01–0.66 eV in $\text{Li}_{13}\text{Si}_4$ and 0.00–0.52 eV in $\text{Li}_{15}\text{Si}_4$. These ranges cover energy barriers computed by Wang *et al* [38], as well as Moon *et al* [45], and they enable diffusion in all four compounds. In Li_1Si_1 , paths (6)_def, (7)_def and (8)_def are three crystallographically distinct jumps of a Li1 atom into an adjacent Li1 vacancy with increasing distances. Migration energies are 0.22 eV, 0.25 eV and 0.28 eV for jump distances of 2.2 Å, 2.7 Å and 2.8 Å, respectively. In $\text{Li}_{12}\text{Si}_7$, path (34)_def is the migration of 3 Li atoms between a Li8 and a Li9 vacancy, with energies of 0.12 eV and 0.22 eV. Path (42)_def transforms between a Li8 and a Li12 vacancy via 4 Li atoms, with migration energies of 0.22 eV and 0.05 eV. In $\text{Li}_{13}\text{Si}_4$, path (45)_def converts a Li1 vacancy into a distributed Li2 vacancy by a movement of 3 Li atoms onto metastable positions, with the migration energy being as low as 0.01 eV. Gruber *et al* obtained a comparably low Li1/Li2 vacancy migration barrier of 0.08 eV [41]. Paths (55)_def and (56)_def couple vacancy jumps to collective chain-like motions to exchange a Li vacancy between two different Li1/Li2 rows. With energy barriers of 0.24 eV and 0.31 eV, these paths mediate Li diffusivity in y - and z -direction as already discussed. In $\text{Li}_{15}\text{Si}_4$, paths (68)_def to (75)_def are jumps of a Li1 atom into a Li1 vacancy. With increasing distances from 2.0 Å to 3.5 Å, migration energies rise from 0.08 eV to 0.52 eV. Vacancy motion between Li1 and Li2 is described by paths (76)_def to (80)_def, with migration barriers increasing from 0.23 eV to 0.32 eV for distances between 2.3 Å and 2.5 Å ($\text{Li2} \rightarrow v_{\text{Li1}}$).

Migration energy barriers in Li_xSi_y systems containing a Li vacancy are compared against those of the same paths in defect-free systems in figure 4. In figure 4(a), migration energies of an isolated Li vacancy are plotted against those of a Frenkel Li vacancy. Data points are on the identity line for Li_1Si_1 , $\text{Li}_{12}\text{Si}_7$ and $\text{Li}_{15}\text{Si}_4$, above it for $\text{Li}_{12}\text{Si}_7$ and below it for Li_1Si_1 and $\text{Li}_{13}\text{Si}_4$. It was already discussed in section 3.1 why $\text{Li}_{15}\text{Si}_4$ is more on line than the other three compounds. Generally, diffusion of an isolated Li vacancy tends to have similar energy barriers to a Frenkel vacancy in the low energy region, and smaller barriers for high energies. A linear fit yields an absolute increase in energy of +0.06 eV, that is primarily important for low energies, and a relative decrease of 40%, that impacts large energies more. In figure 4 (b), only four data points from two migration paths in $\text{Li}_{12}\text{Si}_7$ can be analysed. Three out of four are above the identity line, revealing a potential hindering effect of Li vacancies on nearby pathways, with migration energies increasing by up to +0.2 eV. In figure 4(c), data points are around the identity line with a medium spread of ca. 0.15 eV. A linear fit gives an average decrease in energy of 12% for paths more than 3 Å from the vacancy. Compared



to interstitial Li atoms, migration barriers show similar trends for Li vacancies, with the effect being larger for diffusion of the vacancy itself, and smaller on surrounding diffusion paths. Note that the number of data points in figures 4(a) and (b) limits the significance of these results.

Elastic moduli of all studied systems can be found in table 4. With introduction of a Li vacancy, bulk moduli decrease by $-0.2 \dots -1.9 \text{ GPa}$ and shear moduli by $-0.1 \dots -1.3 \text{ GPa}$ with respect to the defect-free systems. Thus, the lattice softening effect is comparable for Li vacancies and interstitial Li atoms. Again, this could be correlated with the 12% average decrease in migration energies.

Li vacancy formation energies are presented in table 5. Values are the lowest in $\text{Li}_{12}\text{Si}_7$ and $\text{Li}_{13}\text{Si}_4$ with approximately $0.7\text{--}0.8 \text{ eV}$, higher in Li_1Si_1 (1.0 eV) and highest in $\text{Li}_{15}\text{Si}_4$ with $1.3\text{--}1.5 \text{ eV}$. For $\text{Li}_{12}\text{Si}_7$, these agree well with results from Shi *et al* [40]. All of these formation energies are relatively high compared to Li interstitials, being at least 0.8 eV higher in Li_1Si_1 , 0.9 eV in $\text{Li}_{12}\text{Si}_7$, 1.0 eV in $\text{Li}_{13}\text{Si}_4$ and 1.1 eV in $\text{Li}_{15}\text{Si}_4$. Note that Frenkel pair formation energies are thus largely determined by vacancy formation in crystalline Li_xSi_y . Moreover, both Li interstitial and Li vacancy formation energies are notably smaller in $\text{Li}_{12}\text{Si}_7$ and $\text{Li}_{13}\text{Si}_4$ than in Li_1Si_1 and $\text{Li}_{15}\text{Si}_4$, causing significantly smaller Frenkel defect formation energies. Approximating equilibrium site fractions for vacancies at room temperature using the Boltzmann factor $\exp(-\frac{E_{\text{form}}}{k_B T})$, these are in the order of 10^{-12} , 10^{-13} , 10^{-18} and 10^{-23} for the lowest computed formation energy in $\text{Li}_{12}\text{Si}_7$, $\text{Li}_{13}\text{Si}_4$, Li_1Si_1 and $\text{Li}_{15}\text{Si}_4$, respectively. Taking into account the ratios of interstitial sites to Li atoms per crystallographic site for lowest energy vacancy formation, these are 0.25 in Li_1Si_1 , 0.5 in $\text{Li}_{12}\text{Si}_7$, 1.0 in $\text{Li}_{13}\text{Si}_4$ and 0.5 in $\text{Li}_{15}\text{Si}_4$, so they can consequently be neglected when comparing orders of magnitude of the Boltzmann factors. Site fractions of Li interstitials were approximated as $10^{-4}\text{--}10^{-5}$, and are therefore considerably larger than that of Li vacancies, leading to the conclusion that $[\text{Li}_i] \gg [\text{V}_{\text{Li}}]$ for all four compounds.

In summary, presence of Li vacancies can increase diffusivity in crystalline Li_xSi_y , but it can also leave it unaltered or even lead to a decrease, depending on the compound. Likewise, diffusion (an)isotropy can be affected. Migration of isolated Li vacancies takes place either via single-atom jumps or via simultaneous jumps of at least 3 atoms, with on average lower energy barriers compared to vacancies from Frenkel pairs. Migration energies of nearby paths tend to increase due to a vacancy by up to 0.2 eV , and those of farther paths decrease on average by 12%, potentially caused by a slight lattice softening effect. Existence of close-to-zero energy pathways enables facile Li vacancy diffusion in $\text{Li}_{12}\text{Si}_7$, $\text{Li}_{13}\text{Si}_4$ and $\text{Li}_{15}\text{Si}_4$, but also in Li_1Si_1 there is moderate diffusion with a minimum barrier of 0.22 eV . Overall, while in $\text{Li}_{12}\text{Si}_7$ and $\text{Li}_{13}\text{Si}_4$ diffusion is always high independent of non-stoichiometric defects, vacancies could mediate it in Li_1Si_1 and $\text{Li}_{15}\text{Si}_4$. However, Li vacancy concentrations are low in all four compounds due to high formation energies of minimum $0.7\text{--}1.3 \text{ eV}$.

3.3. Schottky defect in Li_1Si_1

A Schottky defect was studied only for Li_1Si_1 , because its stoichiometry does not change upon defect creation. Li diffusivity is low, comparable to that of a Li vacancy, but not zero as in the defect-free system (see table 3). In Li_1Si_1 , there is only one crystallographic Li and Si site each, so all Li and all Si atoms are equivalent. The defect was introduced by removing a Li and an adjacent Si atom. In the AIMD simulation, the Si vacancy was immobile, while the Li vacancy migrated. Results of NEB calculations of all observed migration paths can be found in table S11 in the supporting information and as Supplementary Data [48]. Additionally, the lowest-energy Li diffusion pathway is illustrated in figure S9(c). Initially, one Li atom jumps into a position

between Li and Si vacancy, partially occupying both lattice sites (path (16)_def). The migration energy for this is 0.23 eV, but 0.49 eV for the reverse process, which leads to the Li atom remaining in this position occupying the Schottky defect. The so created Li vacancy then migrates via single-atom jumps, which is described by pathways (6)_def to (15)_def. Paths (6)_def to (8)_def were already discussed in section 3.2. Their energy barriers between 0.22 eV and 0.29 eV depend on the jump distance and are relatively unaffected when compared to an isolated Li vacancy. Paths (11)_def to (15)_def are nearer to the Si vacancy and thus energetically influenced by it. Their energy profiles are asymmetrical with migration barriers between 0.05 eV and 0.56 eV. With path (17)_def, simultaneous migration of two Li atoms via a vacancy mechanism was also observed, exhibiting migration barriers of 0.30 eV and 0.47 eV. In conclusion, the Li vacancy of the Schottky defect migrates comparably to an isolated vacancy, with barriers being affected near the Si vacancy. According to table 4, bulk and shear modulus of Li_xSi_y decrease by -1.8 GPa and -2.6 GPa, respectively, with introduction of a Schottky defect. This decrease is substantially larger than for a Li vacancy, showing that removal of a Si atom from the Si-Si bonding network degrades mechanical stability to a significant extent. However, Schottky defect formation as such is highly unlikely due to a formation energy of 2.69 eV, see table 5. Compared to an isolated Li vacancy, additional creation of a Si vacancy requires roughly 1.7 eV more. Therefore, concentration of Schottky defects, that is proportional to an $\exp(-\frac{E_{\text{form}}}{2k_B T})$ Boltzmann factor, is in the order of 10^{-23} at room temperature, five orders of magnitude lower than for Li vacancies.

3.4. Summary intrinsic defects and comments on the literature

It can be concluded that Li diffusion in crystalline Li_xSi_y is most frequently mediated by Li interstitials and to some minor degree by Frenkel defects. Interstitial Li atoms exhibit both low formation and migration energies in $\text{Li}_{12}\text{Si}_7$, $\text{Li}_{13}\text{Si}_4$ and $\text{Li}_{15}\text{Si}_4$, while Frenkel pairs do so in $\text{Li}_{12}\text{Si}_7$ and $\text{Li}_{13}\text{Si}_4$ only. Additionally, in $\text{Li}_{13}\text{Si}_4$ another diffusion mechanism mediated by transition to a metastable structure is discussed in [41, 42] and plays an important role. In Li_1Si_1 , Li interstitials show low formation, but high migration energies, and vice versa for Frenkel defects, thus no intrinsic defect offers an option for high Li diffusivity. This conclusion was also drawn by Yao *et al* [44]. Although Li vacancies would exhibit low migration barriers in all four compounds, their formation energies are rather too high to contribute to diffusion. A Schottky defect was studied in Li_1Si_1 only, but an even higher formation energy than for a Li vacancy with comparable migration barriers renders this defect very unlikely to play a role in Li diffusion. Generally, both isolated Li interstitials and vacancies were found to exhibit on average slightly lower migration energy barriers than Frenkel pairs. Moreover, they have a local effect increasing migration barriers of nearby paths and a non-local one decreasing average energy barriers, which can be understood in terms of lattice softening.

Kuhn *et al* performed ^7Li NMR experiments on $\text{Li}_{12}\text{Si}_7$ in two studies [23, 26], obtaining activation energies for Li diffusion of 0.18 eV (quasi 1D process), 0.32 eV and 0.55 eV (two 3D processes). Moreover, they assigned Li mobilities to crystallographic sites, which was supported by computational results from Shi *et al* [40]. In their ^7Li NMR measurements, Dupke *et al* confirmed the results for $\text{Li}_{12}\text{Si}_7$ [24], and further characterized $\text{Li}_{13}\text{Si}_4$ and $\text{Li}_{15}\text{Si}_4$ [25]. They obtained an activation energy of 0.25 eV in $\text{Li}_{15}\text{Si}_4$ and concluded that Li diffusion is close to isotropic in $\text{Li}_{13}\text{Si}_4$ and anisotropic in $\text{Li}_{15}\text{Si}_4$. While the assignment of mobilities to Li sites for $\text{Li}_{12}\text{Si}_7$ agrees with the results presented here as well as in our previous study [42], it should be reconsidered for $\text{Li}_{13}\text{Si}_4$ along with the (an)isotropies, that are characterized as anisotropic in $\text{Li}_{13}\text{Si}_4$ and isotropic in $\text{Li}_{15}\text{Si}_4$ here, which is also more consistent with their crystal systems. These points are discussed in more detail in our previous study [42]. For all three compounds, the experimentally determined activation energies do not single out the dominant intrinsic defect, because our calculations of the various migration barriers show that they are equally low for interstitials, vacancies as well as Frenkel pairs.

Therefore, it is necessary to compare the results presented here to previous computational publications. To our knowledge, only Moon *et al* conducted a comparatively thorough study on various diffusion mechanisms in different Li_xSi_y compounds [45]. They calculated Li interstitial formation energies of 0.46 eV (here: Int1) and 0.15 eV (here: Int2) for Li_1Si_1 and 0.25 eV for $\text{Li}_{15}\text{Si}_4$, respectively, and Li vacancy formation energies of 1.20 eV in Li_1Si_1 as well as 1.37 eV (Li1) and 1.62 eV (Li2) in $\text{Li}_{15}\text{Si}_4$. These values approximately agree with the ones presented here, see table 5. They excluded ring mechanisms for diffusion because of high migration barriers of more than 1.10 eV in Li_1Si_1 and 1.87 eV in $\text{Li}_{15}\text{Si}_4$, which is in accordance with our results, see also [42]. They further computed vacancy migration energies of 0.23 eV, 0.25 eV and 0.27 eV in Li_1Si_1 and at least 0.12 eV in $\text{Li}_{15}\text{Si}_4$, and interstitial diffusion barriers of more than 1.20 eV in Li_1Si_1 . All of these values agree excellently with ours, but then they obtain a direct interstitial migration barrier of 2.38 eV in $\text{Li}_{15}\text{Si}_4$, which is a significant contrast to 0.15 eV calculated in our study for a path of the same mechanism and atomic jump distance. Moreover, Moon *et al* did not consider indirect interstitial (interstitialcy) mechanisms, which yield comparatively low energy barriers here. They concluded that due to high interstitial migration barriers in Li_1Si_1 and $\text{Li}_{15}\text{Si}_4$, diffusion has to be vacancy-mediated and proceeded only with this mechanism for $\text{Li}_{12}\text{Si}_7$ and $\text{Li}_{13}\text{Si}_4$. As outlined above, our results support this statement for the case of Li_1Si_1 ,

but not for $\text{Li}_{12}\text{Si}_7$, $\text{Li}_{13}\text{Si}_4$ and $\text{Li}_{15}\text{Si}_4$, especially with interstitialcy paths being considered. Thus, we disagree that diffusion is dominantly vacancy-mediated, but rather conclude it is mainly interstitial-mediated.

4. Conclusions

We have comprehensively studied defect-mediated Li diffusion in crystalline Li_xSi_y for a variety of intrinsic point defects. We have combined AIMDs simulations with NEB calculations to identify and characterize relevant diffusion paths in the four Zintl-like lithium silicides Li_1Si_1 , $\text{Li}_{12}\text{Si}_7$, $\text{Li}_{13}\text{Si}_4$ and $\text{Li}_{15}\text{Si}_4$. Contrary to previous research, we observe that intrinsic Li diffusivity is mediated by Li interstitials and Frenkel pairs rather than Li vacancies or Schottky defects due to high formation energies of the latter two. In particular, low formation and migration energies are found for both Li interstitials and Frenkel defects in $\text{Li}_{12}\text{Si}_7$ and $\text{Li}_{13}\text{Si}_4$, and only for interstitial Li atoms in $\text{Li}_{15}\text{Si}_4$. Li interstitials migrate via an interstitialcy diffusion mechanism typically involving 2 or 3 atoms. Thus, this mode turns out to be the most relevant one for Li diffusion in the technologically relevant compound $\text{Li}_{15}\text{Si}_4$, that forms in Si anodes upon complete lithiation. Moreover, all studied defects induce two complementary energetic effects: firstly, they locally increase average migration barriers of nearby Li diffusion paths, and secondly, they lower average energy barriers of paths in larger distance, correlated with lattice softening. Our perspective now is to move on to studying extrinsic point defects, aiming at characterizing the influence of doping and impurities on Li diffusion in lithium–silicon compounds. Additionally, the results obtained here for crystalline systems can be combined with future results for amorphous Li_xSi to construct multiscale models for simulating lithium mobility in lithium silicides. Ultimately, these models could help with optimizing the design of silicon anodes.

Data availability statement

The data that support the findings of this study are openly available at the following URL/DOI: <https://doi.org/10.5281/zenodo.14065754>.

Acknowledgments

This project was funded by the Deutsche Forschungsgemeinschaft, project IDs 435886714 and 446879138.

ORCID iDs

Christoph Kirsch  <https://orcid.org/0000-0002-4244-8888>

Daniel Sebastiani  <https://orcid.org/0000-0003-2240-3938>

References

- [1] Tarascon J and Armand M 2001 Issues and challenges facing rechargeable lithium batteries *Nature* **414** 359
- [2] Armand M and Tarascon J 2008 Building better batteries *Nature* **451** 652
- [3] Kasavajjula U, Wang C and Appleby A J 2007 Nano- and bulk-silicon-based insertion anodes for lithium-ion secondary cells *J. Power Sources* **163** 1003
- [4] Huggins R A 2009 *Advanced Batteries - Materials Science Aspects* 1st edn (Springer)
- [5] Schweidler S, de Biasi L, Schiele A, Hartmann P, Brezesinski J and Janek T 2018 Volume changes of graphite anodes revisited: a combined operando x-ray diffraction and in situ pressure analysis study *J. Phys. Chem. C* **122** 8829
- [6] Limthongkul P, Jang Y, Dudney N J and Chiang Y 2003 Electrochemically-driven solid-state amorphization in lithium-silicon alloys and implications for lithium storage *Acta Mater.* **51** 1103
- [7] Obrovac M N and Christensen L 2004 Structural changes in silicon anodes during lithium insertion/extraction *Electrochem. Solid-State Lett.* **7** A93
- [8] Li J and Dahn J R 2007 An in situ X-ray diffraction study of the reaction of Li with crystalline Si *J. Electrochem. Soc.* **154** A156
- [9] Gu M, Wang Z, Connell J G, Perea D E, Lauhon L J, Gao F and Wang C 2013 Electronic origin for the phase transition from amorphous Li_xSi to crystalline $\text{Li}_{15}\text{Si}_4$ *ACS Nano* **7** 6303
- [10] Stearns L A, Gryko J, Diefenbacher J, Ramachandran G K and McMillan P F 2003 Lithium monosilicide (LiSi), a low-dimensional silicon-based material prepared by high pressure synthesis: NMR and vibrational spectroscopy and electrical properties characterization *J. Solid State Chem.* **173** 251
- [11] Nesper R, von Schnering H G and Curda J 1986 $\text{Li}_{12}\text{Si}_7$, eine Verbindung mit trigonal-planaren Si_4 -Clustern und isometrischen Si_5 -Ringern *Chem. Ber.* **119** 3576
- [12] Barvík I 1983 To the magnetic properties of $\text{Li}_{2,33}\text{Si}$ *Czech. J. Phys. B* **33** 1338–46
- [13] Zeilinger M and Fässler T F 2013 Revision of the $\text{Li}_{13}\text{Si}_4$ structure *Acta Cryst. E* **69** i81
- [14] Zeilinger M, Baran V, van Wüllen L, Häussermann U and Fässler T F 2013 Stabilizing the phase $\text{Li}_{15}\text{Si}_4$ through lithium-aluminum substitution in $\text{Li}_{15-x}\text{Al}_x\text{Si}_4$ ($0.4 < x < 0.8$) - single crystal x-ray structure determination of $\text{Li}_{15}\text{Si}_4$ and $\text{Li}_{14.37}\text{Al}_{0.63}\text{Si}_4$ *Chem. Mater.* **25** 4113
- [15] Zeilinger M, Kurylyshyn I M, Häussermann U and Fässler T F 2013 Revision of the Li-Si phase diagram: discovery and single-crystal X-ray structure determination of the high-temperature phase $\text{Li}_{4,11}\text{Si}$ *Chem. Mater.* **25** 4623
- [16] Nesper R and von Schnering H G 1987 $\text{Li}_{21}\text{Si}_5$, a Zintl phase as well as a Hume-Rothery phase *J. Solid State Chem.* **70** 48

- [17] Zeilinger M, Benson D, Häussermann U and Fässler T F 2013 Single crystal growth and thermodynamic stability of $\text{Li}_{17}\text{Si}_4$ *Chem. Mater.* **25** 1960
- [18] Gladyshevskii E, Oleksiv G and Kripyakevich P I 1964 New examples of the structural type $\text{Li}_{22}\text{Pb}_5$ *Kristallografiya* **9** 338
- [19] Nesper R 1990 Structure and chemical bonding in Zintl-phases containing lithium *Prog. Solid State Chem.* **20** 1
- [20] Chevrier V, Zwanziger J and Dahn J 2010 First principles study of Li-Si crystalline phases: charge transfer, electronic structure and lattice vibrations *J. Alloys Compd.* **496** 25
- [21] Mehrer H 2007 *Diffusion in Solids - Fundamentals, Methods, Materials, Diffusion-Controlled Processes* 1st edn (Springer)
- [22] Wen C J and Huggins R A 1981 Chemical diffusion in intermediate phases in the lithium-silicon system *J. Solid State Chem.* **37** 271
- [23] Kuhn A, Sreeraj P, Pöttgen R, Wiemhöfer H-D, Wilkening M and Heitjans P 2011 Li ion diffusion in the anode material $\text{Li}_{12}\text{Si}_7$: ultrafast quasi-1D diffusion and two distinct fast 3D jump processes separately revealed by ^7Li NMR relaxometry *J. Am. Chem. Soc.* **133** 11018
- [24] Dupke S, Langer T, Pöttgen R, Winter M and Eckert H 2012 Structural and dynamic characterization of $\text{Li}_{12}\text{Si}_7$ and $\text{Li}_{12}\text{Ge}_7$ using solid state NMR *Solid State Nucl. Magn. Reson.* **42** 17
- [25] Dupke S, Langer T, Pöttgen R, Winter M, Passerini S and Eckert H 2012 Structural characterization of the lithium silicides $\text{Li}_{15}\text{Si}_4$, $\text{Li}_{13}\text{Si}_4$, and Li_7Si_3 using solid state NMR *Phys. Chem. Chem. Phys.* **14** 6496
- [26] Kuhn A, Dupke S, Kunze M, Puravankara S, Langer T, Pöttgen R, Winter M, Wiemhöfer H-D, Eckert H and Heitjans P 2014 Insight into the Li ion dynamics in $\text{Li}_{12}\text{Si}_7$: combining field gradient nuclear magnetic resonance, one- and two-dimensional magic-angle spinning nuclear magnetic resonance and nuclear magnetic resonance relaxometry *J. Phys. Chem. C* **118** 28350
- [27] Ding N, Xu J, Yao Y, Wegner G, Fang X, Chen C and Lieberwirth I 2009 Determination of the diffusion coefficient of lithium ions in nano-Si *Solid State Ion.* **180** 222
- [28] Strauß F, Hüger E, Julin J, Munnik F and Schmidt H 2020 Lithium diffusion in ion-beam sputter-deposited lithium-silicon layers *J. Phys. Chem. C* **124** 8616
- [29] Wang Z et al 2013 Electron-rich driven electrochemical solid-state amorphization in Li-Si alloys *Nano Lett.* **13** 4511
- [30] Wan W, Zhang Q, Cui Y and Wang E 2010 First principles study of lithium insertion in bulk silicon *J. Phys.: Condens. Matter* **22** 415501
- [31] Kim H, Kweon K E, Chou C-Y, Ekerdt J G and Hwang G S 2010 On the nature and behavior of Li atoms in Si: a first principles study *J. Phys. Chem. C* **114** 17942
- [32] Chou C-Y, Kim H and Hwang G S 2011 A comparative first-principles study of the structure, energetics and properties of Li-M (M = Si, Ge, Sn) alloys *J. Phys. Chem. C* **115** 20018
- [33] Malvi O I, Tan T L and Manzhos S 2013 A comparative computational study of structures, diffusion and dopant interactions between Li and Na insertion into Si *Appl. Phys. Express* **6** 027301
- [34] Halder P and Chatterjee A 2014 Nudged-elastic band study of lithium diffusion in bulk silicon in the presence of strain *Energy Proc.* **54** 310
- [35] Wang Z, Su Q, Deng H, He W, Lin J and Fu Y Q 2014 Modelling and simulation of electron-rich effect on Li diffusion in group IVA elements (Si, Ge and Sn) for Li ion batteries *J. Mater. Chem. A* **2** 13976
- [36] Yan X, Gouissem A and Sharma P 2015 Atomistic insights into Li-ion diffusion in amorphous silicon *Mech. Mater.* **91** 306
- [37] Johari P, Qi Y and Shenoy V B 2011 The mixing mechanism during lithiation of Si negative electrode in Li-ion batteries: an *ab initio* molecular dynamics study *Nano Lett.* **11** 5494
- [38] Wang Z, Su Q, Deng H and Fu Y 2015 Composition dependence of lithium diffusion in lithium silicide: a density functional theory study *ChemElectroChem* **2** 1292
- [39] Kim H, Chou C-Y, Ekerdt J G and Hwang G S 2011 Structure and properties of Li-Si alloys: a first-principles study *J. Phys. Chem. C* **115** 2514
- [40] Shi J, Wang Z and Fu Y 2015 Atomistic study of lithium ion dynamics in $\text{Li}_{12}\text{Si}_7$ *Electrochim. Acta* **186** 71
- [41] Gruber T, Bahmann S and Kortus J 2016 Metastable structure of $\text{Li}_{13}\text{Si}_4$ *Phys. Rev. B* **93** 144104
- [42] Kirsch C, Dreßler C and Sebastiani D 2022 Atomistic diffusion pathways of lithium ions in crystalline lithium silicides from *ab initio* molecular dynamics simulations *J. Phys. Chem. C* **126** 12136
- [43] Wang Q, Cui W, Xu W, Gao K, Hao J, Shi J, Liu H and Li Y 2024 Pressure-stabilized electride Li_{10}Si with superconducting and superionic behavior *Phys. Rev. B* **110** 134114
- [44] Yao H R, Wang Z Q, Wu M S, Liu G, Lei X L, Xu B, Le J X and Ouyang C Y 2014 Lithium ion migration in Li-Si alloys: from first principles studies *Int. J. Electrochem. Sci.* **9** 1854
- [45] Moon J, Lee B, Cho M and Cho K 2016 *Ab initio* and kinetic Monte Carlo study of lithium diffusion in LiSi , $\text{Li}_{12}\text{Si}_7$, $\text{Li}_{13}\text{Si}_5$ and $\text{Li}_{15}\text{Si}_4$ *J. Power Sources* **328** 558
- [46] Momma K and Izumi F 2011 VESTA3 for three-dimensional visualization of crystal, volumetric and morphology data *J. Appl. Crystallogr.* **44** 1272
- [47] Humphrey W, Dalke A and Schulten K 1996 VMD: visual molecular dynamics *J. Mol. Graph.* **14** 33
- [48] Kirsch C, Dreßler C, and Sebastiani D 2024 Supplementary data for “Li+ diffusion in crystalline lithium silicides: influence of intrinsic point defects *Zenodo* <https://doi.org/10.5281/zenodo.14065754>
- [49] Jiang C, Maloy S and Srinivasan S 2008 A computational method to identify interstitial sites in complex materials *Scr. Mater.* **58** 739
- [50] Hohenberg P and Kohn W 1964 Inhomogeneous electron gas *Phys. Rev.* **136** B864
- [51] Kohn W and Sham L J 1965 Self-consistent equations including exchange and correlation effects *Phys. Rev.* **140** A1133
- [52] Hutter J, Iannuzzi M, Schiffmann F and VandeVondele J 2014 cp2k: atomistic simulations of condensed matter systems *Wiley Interdiscip. Rev.-Comput. Mol. Sci.* **4** 15
- [53] Kühne T D et al 2020 CP2K: an electronic structure and molecular dynamics software package - quickstep: efficient and accurate electronic structure calculations *J. Chem. Phys.* **152** 194103
- [54] VandeVondele J, Krack M, Mohamed F, Parrinello M, Chassaing T and Hutter J 2005 Quickstep: fast and accurate density functional calculations using a mixed Gaussian and plane waves approach *Comput. Phys. Commun.* **167** 103
- [55] Lippert G, Hutter J and Parrinello M 1997 A hybrid Gaussian and plane wave density functional scheme *Mol. Phys.* **92** 477
- [56] VandeVondele J and Hutter J 2007 Gaussian basis sets for accurate calculations on molecular systems in gas and condensed phases *J. Chem. Phys.* **127** 114105
- [57] Goedecker S, Teter M and Hutter J 1996 Separable dual-space Gaussian pseudopotentials *Phys. Rev. B* **54** 1703
- [58] Hartwigsen C, Goedecker S and Hutter J 1998 Relativistic separable dual-space Gaussian pseudopotentials from H to Rn *Phys. Rev. B* **58** 3641

- [59] Krack M 2005 Pseudopotentials for H to Kr optimized for gradient-corrected exchange-correlation functionals *Theor. Chem. Acc.* **114** 145
- [60] Perdew J P, Burke K and Ernzerhof M 1996 Generalized gradient approximation made simple *Phys. Rev. Lett.* **77** 3865
- [61] Perdew J P, Burke K and Ernzerhof M 1997 Generalized gradient approximation made simple [Phys. Rev. Lett. 77, 3865 (1996)] *Phys. Rev. Lett.* **78** 1396
- [62] Grimme S, Antony J, Ehrlich S and Krieg H 2010 A consistent and accurate ab initio parametrization of density functional dispersion correction (DFT-D) for the 94 elements H-Pu *J. Chem. Phys.* **132** 154104
- [63] Broyden C G 1965 A class of methods for solving nonlinear simultaneous equations *Math. Comput.* **19** 577
- [64] Mermin N D 1965 Thermal properties of the inhomogeneous electron gas *Phys. Rev.* **137** A1441
- [65] Broyden C G 1970 The convergence of a class of double-rank minimization algorithms 1. General considerations *IMA J. Appl. Math.* **6** 76
- [66] Fletcher R 1970 A new approach to variable metric algorithms *Comput. J.* **13** 317
- [67] Goldfarb D 1970 A family of variable-metric methods derived by variational means *Math. Comput.* **24** 23
- [68] Shanno D F 1970 Conditioning of quasi-Newton methods for function minimization *Math. Comput.* **24** 647
- [69] Nosé S 1984 A molecular dynamics method for simulations in the canonical ensemble *Mol. Phys.* **52** 255
- [70] Nosé S 1984 A unified formulation of the constant temperature molecular dynamics methods *J. Chem. Phys.* **81** 511
- [71] Henkelman G, Uberuaga B P and Jónsson H 2000 A climbing image nudged elastic band method for finding saddle points and minimum energy paths *J. Chem. Phys.* **113** 9901
- [72] Mills G and Jónsson H 1994 Quantum and thermal effects in H₂ dissociative adsorption: evaluation of free energy barriers in multidimensional quantum systems *Phys. Rev. Lett.* **72** 1124
- [73] Mills G, Jónsson H and Schenter G K 1995 Reversible work transition state theory: application to dissociative adsorption of hydrogen *Surf. Sci.* **324** 305
- [74] Berne B J, Ciccotti G and Coker D F 1998 *Classical and Quantum Dynamics in Condensed Phase Simulations* 1st edn (World Scientific)
- [75] Henkelman G and Jónsson H 2000 Improved tangent estimate in the nudged elastic band method for finding minimum energy paths and saddle points *J. Chem. Phys.* **113** 9978
- [76] Monkhorst H J and Pack J D 1976 Special points for Brillouin-zone integrations *Phys. Rev. B* **13** 5188
- [77] Freysoldt C, Grabowski B, Hickel T, Neugebauer J, Kresse G, Janotti A and Van de Walle C G 2014 First-principles calculations for point defects in solids *Rev. Mod. Phys.* **86** 253
- [78] de Jong M et al 2015 Charting the complete elastic properties of inorganic crystalline compounds *Sci. Data* **2** 1
- [79] Braga M H, Debski A and Gasior W 2014 Li-Si phase diagram: enthalpy of mixing, thermodynamic stability and coherent assessment *J. Alloys Compd.* **616** 581